

# Spontaneous Crystallization of Skyrmions and Fractional Vortices in the Fast-rotating and Rapidly-quenched Spin-1 Bose-Einstein Condensates

S.-W. Su,<sup>1</sup> C.-H. Hsueh,<sup>2</sup> I.-K. Liu,<sup>3</sup> T.-L. Horng,<sup>4</sup> Y.-C. Tsai,<sup>5</sup> S.-C. Gou,<sup>3</sup> and W. M. Liu<sup>6</sup>

<sup>1</sup>*Department of Physics, National Tsing Hua University, Hsinchu 30013, Taiwan*

<sup>2</sup>*Department of Physics, National Taiwan Normal University, Taipei 11677, Taiwan*

<sup>3</sup>*Department of Physics, National Changhua University of Education, Changhua 50058, Taiwan*

<sup>4</sup>*Department of Applied Mathematics, Feng Chia University, Taichung 40724, Taiwan*

<sup>5</sup>*Department of Photonics, Feng Chia University, Taichung 40724, Taiwan*

<sup>6</sup>*Institute of Physics, Chinese Science Academy, Beijing 100190, P. R. China*

(Dated: May 20, 2011)

We investigate the spontaneous generation of crystallized topological defects via the combining effects of fast rotation and rapid thermal quench on the spin-1 Bose-Einstein condensates. By solving the stochastic projected Gross-Pitaevskii equation, we show that, when the system reaches equilibrium, a hexagonal lattice of skyrmions, and a square lattice of half-quantized vortices can be formed in a ferromagnetic and antiferromagnetic spinor BEC, respectively, which can be imaged by using the polarization-dependent phase-contrast method.

PACS numbers: 03.75.Lm, 03.75.Mn, 03.75.Kk, 05.10.Gg

Topological defects are a manifestation of spontaneously broken symmetries [1]. Formation and observation of topological defects are one of the most fundamental and fascinating topics in various aspects of physics, ranging from condensed matter physics to cosmology. However, owing to the limitation of energy scales in the earth-bound physics experiments, topological defects are mostly created and observed in the condensed matter systems. For example, magnetic domain walls of magnetized material and string defects in <sup>3</sup>He superfluid phase transitions have been extensively studied [2].

Recently, owing to the realization of spinor Bose-Einstein condensate (BEC) of alkali atoms in optical trap [3, 4], the creation of topological defects in ultracold atomic systems has become possible. A spinor BEC is fully characterized by the spin degrees of freedom and behaves as a vector in the spin space. Theoretical studies for the spinor BEC were pioneered by Ho [5], and independently by Ohmi and Machida [6]. More recently, spinor BECs with  $F > 1$  [7–9] or with long range dipolar interaction [10, 11] have also been theoretically investigated. In general, the physical behavior of the spinor BEC depends crucially on its magnetic properties, such that the interplay between the superfluidity and magnetism of the condensate makes the spinor BEC a candidate to exhibit a variety of nontrivial ordered states, such as the skyrmions [12], Mermin-Ho vortices [13], Anderson-Thouless vortices [14] and so forth.

So far, all theoretical studies regarding the formation of topological defects in spinor BEC appeal to manipulate the external and internal degrees of freedom of the condensed atoms at zero temperature. On the other hand, according to the Kibble-Zurek scenario, topological defects can also be created through phase transitions at finite temperatures, which are fundamentally caused by spontaneous symmetry breaking and thermal fluctuations near the critical point. In this paper, we show that it is possible to create crystalline orders of skyrmions

and fractional vortices simply by thermally quenching a rotating spin-1 BEC. This enables us to probe into the very fundamental aspects of topological defects without any engineering of dynamical processes, since evaporative cooling is prerequisite in creating BECs and the methods of rotating condensates have been well developed in a variety of ultracold atoms experiments. In the framework of mean field theory, the dynamics of a BEC at nonzero temperatures can be described by the stochastic projected Gross-Pitaevskii equation (SPGPE) [15], which relies on the assumption that the system can be treated as a condensate band in contact with a thermal reservoir comprising of all non-condensed particles. In such a scheme, the condensate band is described by the truncated Wigner method [16] including the projected c-field method, while the non-condensate band is described by the quantum kinetic theory [17, 18]. In the following, we shall solve the SPGPE numerically for a rotating trapped spin-1 BEC. We show that when the system is quenched down to a very low temperature, a lattice of skyrmions and half-quantized vortices (HQVs) can be created in the spinor BEC of <sup>87</sup>Rb and <sup>23</sup>Na, respectively.

The spin-1 BEC is characterized by a vectorial order parameter,  $\Psi = (\Psi_1, \Psi_0, \Psi_{-1})^T$  (the superscript  $T$  stands for the transpose), where  $\Psi_j$  ( $j = \pm 1, 0$ ) denotes the macroscopic wave function of the atoms condensed in the spin states,  $|F = 1, m_F = \pm 1, 0\rangle$ , respectively. The dynamics of  $\Psi_j$  in a confining potential is described by the following coupled nonlinear Schrödinger equations

$$i\hbar\partial_t\Psi_j = \hat{H}_j^{GP}\Psi_j \quad (1)$$

$$= \mathcal{H}\Psi_j + g_s \sum_{\alpha=x,y,z} \sum_{n,k,l=0,\pm 1} \left(\hat{F}_\alpha\right)_{jn} \left(\hat{F}_\alpha\right)_{kl} \Psi_n \Psi_k^* \Psi_l$$

where  $\mathcal{H} = -\hbar^2\nabla^2/2m + V(\mathbf{r}) + g_n|\Psi|^2$  denotes the spin-independent part of the Hamiltonian, and  $\hat{F}_\alpha$  are the matrices representing the Cartesian components of the spin

angular momentum with quantization axis fixed in the  $z$ -axis. The coupling constants  $g_n$  and  $g_s$  characterizing the density-density and spin-exchange interactions, respectively, are related to the  $s$ -wave scattering lengths  $a_0$  and  $a_2$  in the total spin channels  $F_{total} = 0$  and  $F_{total} = 2$  by  $g_n = 4\pi\hbar^2(a_0 + 2a_2)/3m$ ,  $g_s = 4\pi\hbar^2(a_2 - a_0)/3m$  [5, 6]. The ground state of the spinor BEC depends crucially on the sign of  $g_s$ . For the *ferromagnetic* coupling,  $g_s < 0$ , the condensate is in the “axial” state,  $|\langle \hat{\mathbf{F}} \rangle| = 1$  [5]. On the other hand, for the *antiferromagnetic* coupling,  $g_s > 0$ , the condensate is in the “polar” state,  $\langle \hat{\mathbf{F}} \rangle = 0$  [5]. As we shall focus on the vortices formed by the spin textures, it is more convenient to introduce the basis set  $\Psi_\alpha$  ( $\alpha = x, y, z$ ), such that  $\Psi_{\pm 1} = (\pm\Psi_x + i\Psi_y)/\sqrt{2}$  and  $\Psi_0 = \Psi_z$ . As a result,  $\hat{F}_\alpha|\alpha\rangle = 0$ , and the spin texture, which is parallel to the local magnetic moment, is defined by  $\mathbf{S}(\mathbf{r}) = i\rho^{-1}\tilde{\Psi}^\dagger \times \tilde{\Psi}$  where  $\tilde{\Psi} = (\Psi_x, \Psi_y, \Psi_z)^T$  [19]. Consequently, we have  $S_x \propto \text{Re}[(\Psi_1 + \Psi_{-1})\Psi_0^*]$ ,  $S_y \propto \text{Re}[i(\Psi_1 - \Psi_{-1})\Psi_0^*]$ , and  $S_z \propto |\Psi_1|^2 - |\Psi_{-1}|^2$ . For later convenience, we define the unit vector  $\mathbf{s}(\mathbf{r}) = \mathbf{S}(\mathbf{r})/|\mathbf{S}(\mathbf{r})|$ .

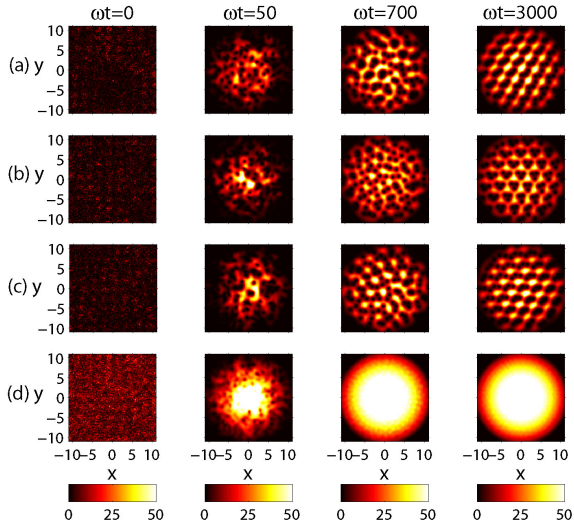


FIG. 1: (Color online) Snapshots of (a)  $|\Psi_{-1}|^2$ ; (b)  $|\Psi_0|^2$ ; (c)  $|\Psi_1|^2$ ; (d)  $|\Psi|^2$  for the quenched rotating spinor BEC of  $^{87}\text{Rb}$ . When the system reaches equilibrium at  $T = 10$  nK with  $\Omega = 0.95$ ,  $\mu = 8$  (rightmost column), crystalline order of vortex-trimers is established in each  $\Psi_j$ . The particle numbers in the spinor BEC are  $N_{\pm 1} \approx 4.84 \times 10^3$ ,  $N_0 \approx 4.79 \times 10^3$ .

To study the non-equilibrium dynamics of a quenched rotating spinor BEC, we shall generalize the formulae in Ref.[15] to the following set of coupled SPGPEs

$$\begin{aligned} & \partial_t \Psi_j \\ &= \mathcal{P} \left\{ -\frac{i}{\hbar} \hat{H}_j^{GP} \Psi_j + \frac{\gamma_j}{k_B T} \left( \mu - \hat{H}_j^{GP} \right) \Psi_j + \frac{dW_j}{dt} \right\} \end{aligned} \quad (2)$$

where  $T$  and  $\mu$  denote the final temperature and chemical potential,  $\gamma_j$  the growth rate for the  $j$ -th component,

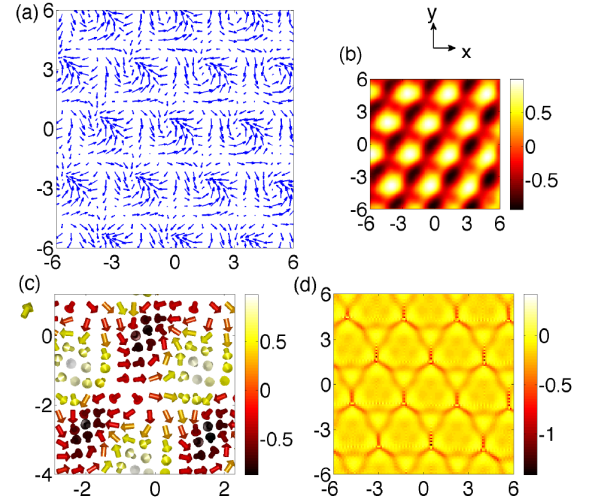


FIG. 2: (Color online) (a) The equilibrium spin textures for the spinor BEC of  $^{87}\text{Rb}$ ; (b) Distribution of  $S_z$  in the spin textures; (c) The orientations of the unit vector  $\mathbf{s}(\mathbf{r})$  for a skyrmion. The color of each arrow indicates the magnitude of  $S_z$ ; (d) The density profile of the topological charges.

and  $dW_j/dt$  is the complex-valued white noise associated with the condensate growth. The projection operator  $\mathcal{P}$  restricts the dynamics of the spinor BEC in the lower energy region below the cutoff energy  $E_R$ . In the rotating frame,  $\hat{\mathcal{H}}$  is replaced by  $\hat{\mathcal{H}} - \Omega \hat{L}_z$ , where  $\hat{L}_z = -i\hbar(x\partial_y - y\partial_x)$  is the  $z$ -component of the orbital angular momentum, and  $\Omega$  is the angular frequency of rotation. As we shall focus on the fast rotating BECs, in which the atomic cloud appears highly pancake-shaped, it is reasonable to treat the system as two-dimensional. We therefore assume  $V(\mathbf{r}) = m\omega^2(x^2 + y^2 + \lambda^2 z^2)/2$  with  $\lambda \gg 1$ . The effective 2D interaction strength can be obtained by integrating the wave functions with respect to  $z$  to eliminate the axial degree of freedom. The numerical procedures for integrating the set of coupled SPGPEs, are described as follows. First, the initial state of each  $\Psi_j$  is sampled by using the grand-canonical ensemble for free ideal Bose gas at a temperature  $T_0$  below the critical temperature and of chemical potentials  $\mu_{j,0}$ . The spatial dependence of the initial state can be specified as a linear combination of some basis functions. Here, we adopt the basis consisted of plane waves with quantized momentum  $\mathbf{k} = 2\pi(n_x, n_y)/L$  ( $n_x, n_y$  are integers and  $L$  is the size of the computation domain), i.e.,  $\Psi_j(t=0) = \sum_{\mathbf{k}}^{E_R} a_{j,\mathbf{k}} \psi_{\mathbf{k}}(\mathbf{r})$ , where  $\psi_{\mathbf{k}}(\mathbf{r})$  are the plane-wave basis functions. The condensate band lies below the an energy cutoff  $E_R > E_{\mathbf{k}} = \hbar^2|\mathbf{k}|^2/2m$ . Furthermore, the distribution is sampled by  $a_{j,\mathbf{k}} = (N_{j,\mathbf{k}} + 1/2)^{1/2} \eta_{j,\mathbf{k}}$  where  $N_{j,\mathbf{k}} = [\exp((E_{j,\mathbf{k}} - \mu_{j,0})/k_B T_0) - 1]^{-1}$  and  $\eta_{j,\mathbf{k}}$  are the complex Gaussian random variables with moments  $\langle \eta_{j,\mathbf{k}} \eta_{j,\mathbf{k}'} \rangle = \langle \eta_{j,\mathbf{k}}^* \eta_{j,\mathbf{k}'}^* \rangle = 0$  and  $\langle \eta_{j,\mathbf{k}} \eta_{j,\mathbf{k}'}^* \rangle = \delta_{\mathbf{k}\mathbf{k}'}$ . Second, to simulate the thermal quench, the tem-

perature and chemical potential of the non-condensate band are altered to the new values  $T < T_0$  and  $\mu > \mu_{j,0}$ . For convenience, we adopt the oscillator units in the numerical computations, where the length, time and energy are respectively scaled in units of  $\sqrt{\hbar/m\omega}$ ,  $\omega^{-1}$  and  $\hbar\omega$ .

We first study the spinor BEC of  $^{87}\text{Rb}$ , which has a  $g_s < 0$ . The total number of the modes are  $n_x, n_y = 256$  and the energy cutoff is chosen at  $n_{xc}, n_{yc} = 128$ . The parameters are  $\Omega = 0.95$ ,  $T = 10\text{nK}$ ,  $\mu = 8$ , and  $\hbar\gamma_j/k_B T = 0.03$  for all  $\Psi_j$ 's. The time evolutions of the density profiles for  $\Psi_j$ 's are shown in Fig.1. During the evaporative cooling, the rotating condensates grow up and the emergent vortices start closely binding up and forming vortex-trimers in each  $\Psi_j$ . When the system reaches equilibrium, these vortex-trimers arrange themselves into some interwoven lattice structures such that each vortex core of  $\Psi_j$  is filled up with particles of the rest two components. In other words, quantized vortices of either inter- or intraspecies, avoid to overlap with each other. The shapes of the trimer structures in all components are somewhat different. To characterize these structures, we calculate the incompressible kinetic energy per particle for each  $\Psi_j$ . This can be done by writing  $\Psi_j = |\Psi_j| \exp(i\varphi_j)$  and defining the current  $\mathbf{Z}_j = |\Psi_j| \nabla \varphi_j = \mathbf{Z}_j^{(i)} + \mathbf{Z}_j^{(c)}$  [20] in terms of the solenoidal and irrotational fields, where  $\nabla \cdot \mathbf{Z}_j^{(i)} = 0$ ,  $\nabla \times \mathbf{Z}_j^{(c)} = 0$ . The incompressible energy is defined by  $\mathcal{E}_{k,j}^{(i)} = (1/2) \int d^2r |\mathbf{Z}_j^{(i)}|^2$ , which corresponds to the kinetic energy of swirls in the superflows. Consequently, we find that  $\mathcal{E}_{k,j}^{(i)}/N_j = 19.48, 19.27, 20.05$  for  $j = \pm 1, 0$ , respectively. The spin textures are shown in Fig.2(a), where a hexagonal lattice is visualized. Furthermore, the spatial variation of the local spin moments parallel to the axis of rotation is plotted in Fig.2(b). An enlarged perspective view of the 3-dimensional orientations of the local spins is shown in Fig.2(c). Taking the island around the trap center for example, we see that the innermost spin points into the paper, while the others increasingly twist and bend in upwards direction. This vortex-like arrangement of magnetic moments is exactly the configuration of a skyrmion [21–23]. Since the central spin in the skyrmion is perpendicular to the rotating plane,  $S_x$  and  $S_y$  must vanish therein, implying that the skyrmions must be centered at the regions of  $\Psi_0 = 0$ , i.e., the cores of the vortex-trimer in  $\Psi_0$ . The topological charge density,  $\sigma = \mathbf{s} \cdot (\partial \mathbf{s} / \partial x \times \partial \mathbf{s} / \partial y) / 4\pi$  [22], is shown in Fig.2(d), which exhibits a hexagonal lattice structure. Numerical integration over the primitive unit cell reveals that each skyrmion carries a topological charge  $Q = -1$ . We notice that the crystallization of skyrmions have recently been observed in various magnetic materials characterized by the Dzyaloshinskii-Moriya interaction [22, 23]. Amazingly, the spin textures in these magnetic materials are highly resembling to those in Fig.2(a).

For the case of  $g_s > 0$ , we consider the spinor BECs of  $^{23}\text{Na}$ . We set  $\Omega = 0.8$ ,  $T = 10\text{ nK}$ ,  $\mu = 25$ , and

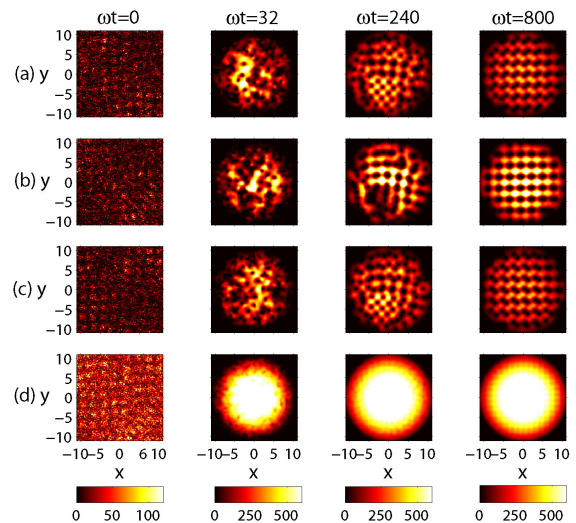


FIG. 3: (Color online) Snapshots of (a)  $|\Psi_{-1}|^2$ ; (b)  $|\Psi_0|^2$ ; (c)  $|\Psi_1|^2$ ; (d)  $|\Psi|^2$  for a quenched rotating spinor BEC of  $^{23}\text{Na}$ . When the system reaches equilibrium at  $T = 10\text{ nK}$  with  $\Omega = 0.8$ ,  $\mu = 25$  (rightmost column), crystalline order of vortex-dimers is established in each  $\Psi_j$ . The particle numbers in the spinor BEC are  $N_{\pm 1} \approx 4.55 \times 10^4$ ,  $N_0 \approx 7.70 \times 10^4$ .

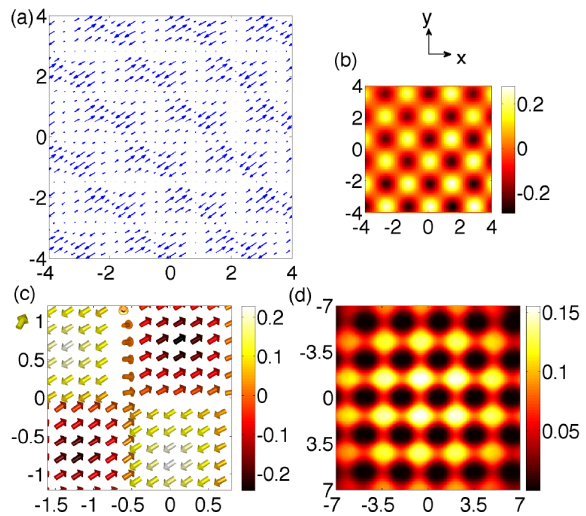


FIG. 4: (Color online) (a) The equilibrium spin textures for the spinor BEC of  $^{23}\text{Na}$ ; (b) Distribution of  $S_z$  in the spin textures; (c) The orientations of the unit vector  $\mathbf{s}(\mathbf{r})$  in the adjacent magnetic domains. The color of each arrow indicates the magnitude of  $S_z$ ; (d) The modulus of  $|\Psi_1 - e^{-2i\phi(\mathbf{r})}\Psi_{-1}|$ , where dark shaded regions reveal the locations of HQVs.

$\hbar\gamma_j/k_B T = 0.03$  for all spin components. The total number of modes and energy cutoff remain the same as those for the case of  $^{87}\text{Rb}$ . In Fig.3, the time evolutions of the density profiles for  $\Psi_j$  are shown. The nucleation of the vortices in the current case are similar to that of the case of  $^{87}\text{Rb}$ , except that a square lattice

of tightly bound vortex-dimers is formed in each component. Consequently, we find that  $\mathcal{E}_{k,j}^{(i)}/N_j = 13.44, 13.45, 12.54$  for  $j = \pm 1, 0$ , respectively. The equilibrated spin textures on the rotating plan are shown in Fig.4(a), in which a mosaic of magnetic domains with staggered magnetization is created. In Fig.4(b) and (c), we see that almost all spins in the magnetic domains lie in the  $xy$ -plane. Spins belonging to the same domain align nearly unidirectionally. Note that the spins reverse their magnetization through a Bloch wall transition in a very narrow region near the boundary between two adjacent domains. These staggered magnetic domains act as the smoking gun of HQVs which have been predicted to exist in superfluid  $^3\text{He}$  [2] and superconductors [24]. Considering the transformation,  $\Psi \rightarrow \hat{G}(\theta) \hat{R}(\mathbf{n}, \chi) \Psi$ , where  $\hat{G}(\theta) = \exp(i\theta)$  is a gauge transformation and  $\hat{R}(\mathbf{n}, \chi) = \exp(i\chi \mathbf{n} \cdot \hat{\mathbf{F}})$  is a spin rotation through an angle  $\chi$  about the unit vector  $\mathbf{n}$ , a HQV entails a spin rotation with  $\chi = \pi$  followed by a global phase change of  $\pi$  in  $\Psi$ . Without loss of generality, we assume  $s(\mathbf{r}) = \cos \phi(\mathbf{r}) \mathbf{e}_x + \sin \phi(\mathbf{r}) \mathbf{e}_y$ . Numerically, we verify that the spin textures remain unchanged through the transformation  $\hat{G}(\pi) \hat{R}(\mathbf{s}, \pi) \Psi = (e^{-2i\phi(\mathbf{r})} \Psi_{-1}, \Psi_0, e^{2i\phi(\mathbf{r})} \Psi_1)^T$ . Upon requiring  $\hat{G}(\pi) \hat{R}(\mathbf{s}, \pi) \Psi = e^{i2\pi} \Psi$ , it follows that  $e^{-2i\phi(\mathbf{r})} \Psi_{-1} = \Psi_1$  and  $e^{2i\phi(\mathbf{r})} \Psi_1 = \Psi_{-1}$ . The redundancy of the last equality implies that there are multiple solutions satisfying the criterion,  $|\Psi_1 - e^{-2i\phi(\mathbf{r})} \Psi_{-1}| = 0$ , or equivalently,  $|\Psi_{-1}| = |\Psi_1|$ . In Fig.4(d), the modulus  $|\Psi_1 - e^{-2i\phi(\mathbf{r})} \Psi_{-1}|$  is plotted where the dark shaded areas represent the core positions of HQVs, which form a square lattice apparently. Likewise, the HQVs are localized at the cores of vortex-dimers in  $\Psi_0$ . Our results are consistent with those obtained by means of dynamical creation [25], where a lattice of HQVs can be created in a rotating optical trap when additional pulsed magnetic trapping potentials are applied. Furthermore, the ground state of a rotating dipolar spinor BEC has been shown to have the same structure when the dipole-dipole interaction is small compared to the contact ones [26].

We note that an  $\Omega$  comparable to  $\omega$  is needed to stabilize the crystalline orders of defects. Under such a fast rotation, the filling factor  $\nu$ , i.e., the ratio of the number of atoms to the number of vortices, can have a value of few hundreds for each component, as shown in Fig.1 and Fig.3. According to the criterion in [27], the system enters the mean-field quantum Hall regime, in which the mean-field theory still applies yet the state of the system can be well described in the lowest Landau level approximation. When  $\Omega$  is not sufficiently large, the crystallization does not arise albeit some few topological defects may be readily created in the condensate. For example, in our simulations with  $\Omega = 0.3$ , we find only a few HQVs nucleating in the spinor BEC of  $^{23}\text{Na}$  during the rapid rotational evaporative cooling. The situation is somewhat different in the case of  $^{87}\text{Rb}$ , where Mermin-Ho vortices, rather than the skyrmions, are created in the condensate. Furthermore, to see whether the crystallization is robust against the thermal fluctuations arising from the growth of condensate, we have assumed a range of final equilibrium temperatures in the simulations. We find that both crystalline orders remain intact for temperatures lower than 50nK. At higher temperatures, however, the crystallization is thwarted by the fluctuations of spin textures so that the lattice becomes disordered and starts melting when the system approaches the critical regime.

In summary, we have investigated the non-equilibrium dynamics of spin-1 BECs during the rapid rotational evaporative cooling. Crystallization of skyrmions and HQVs is predicted to arise in the spinor BEC of  $^{87}\text{Rb}$  and  $^{23}\text{Na}$ , respectively. To resolve the spatial magnetization of the crystallized topological defects, the images have to be taken in situ, and this can be achieved basically by using the polarization-dependent phase-contrast technique [28].

S.-C. Gou is supported by NSC, Taiwan, under Grant No. 98-2112-M-018-001-MY2. W. M. Liu is supported by NSFC under Grant No. 10934010, and NKBRF under Grant No. 2011CB921502.

- 
- [1] G. E. Volovik, *Exotic Properties of Superfluid  $^3\text{He}$*  (World Scientific Singapore, 1992).  
[2] G. E. Volovik, *The Universe in a Helium Droplet* (Clarendon Press, Oxford, 2003).  
[3] D. M. Stamper-Kurn *et al.*, Phys. Rev. Lett. **80**, 2027 (1998).  
[4] M. D. Barrett *et al.*, Phys. Rev. Lett. **87**, 010404 (2001).  
[5] T.-L. Ho, Phys. Rev. Lett. **81**, 742 (1998).  
[6] T. Ohmi and K. Machida, J. Phys. Soc. Jpn. **67**, 1822 (1998).  
[7] M. Ueda *et al.*, Phys. Rev. A **65**, 063602 (2002).  
[8] H. Schmaljohann *et al.*, Phys. Rev. Lett. **92**, 040402 (2004).  
[9] H. Saito *et al.*, Phys. Rev. A **72**, 053628 (2005).  
[10] M. Yasunaga *et al.*, Phys. Rev. Lett. **101**, 220401 (2008).  
[11] S. Hoshi *et al.*, Phys. Rev. A **81**, 013627 (2010).  
[12] U. Al Khawaja *et al.*, Phys. Rev. A **64**, 043612 (2001).  
[13] N. D. Mermin, *et al.*, Phys. Rev. Lett. **36**, 594 (1976).  
[14] P. W. Anderson *et al.*, Phys. Rev. Lett. **38**, 508 (1977).  
[15] A. S. Bradley *et al.*, Phys. Rev. A **77**, 033616 (2008).  
[16] A. Sinatra *et al.*, J. Phys. B **35**, 3599 (2002).  
[17] C. W. Gardiner *et al.*, Phys. Rev. A **58**, 1050 (1998).  
[18] C. W. Gardiner *et al.*, Phys. Rev. A **61**, 033601 (2000).  
[19] T. Mizushima *et al.*, Phys. Rev. A **70**, 043613 (2004).  
[20] T.-L. Horng *et al.*, Phys. Rev. A **80**, 023618 (2009).  
[21] U. K. Röbler *et al.*, Nature **442**, 797 (2006).  
[22] S. Mühlbauer *et al.*, Science **323**, 915 (2009).  
[23] X. Z. Yu *et al.*, Nature **465**, 17 (2010).  
[24] D. A. Ivanov, Phys. Rev. Lett. **86**, 268 (2001).  
[25] A-C Ji *et al.*, Phys. Rev. Lett. **101**, 010402 (2008).

- [26] T. P. Simula *et al.*, J. Phys. Soc. Jpn. **80**, 013001 (2011).      [28] J. M. Higbie *et al.*, Phys. Rev. Lett. **95**, 050401 (2005).  
[27] T.-L. Ho, Phys. Rev. Lett. **87**, 060403 (2001).